

IET Cyber- Systems and Robotics

Special issue Call for Papers

**Be Seen. Be Cited.
Submit your work to a new
IET special issue**

Connect with researchers and experts in your field and share knowledge.

Be part of the latest research trends, faster.

[Read more](#)



The Institution of
Engineering and Technology

Impedance learning adaptive super-twisting control of a robotic exoskeleton for physical human-robot interaction

Brahim Brahmi¹  | Mohammad Habibur Rahman² | Maarouf Saad³

¹Department of Electrical Engineering, College Ahuntsic, Montreal, Quebec, Canada

²Department of Mechanical Engineering, University of Wisconsin-Milwaukee, Milwaukee, WI, USA

³Department of Electrical Engineering, École de Technologie Supérieure, Montreal, Quebec, Canada

Correspondence

Brahim Brahmi, Department of Electrical engineering, College Ahuntsic, Montreal, Quebec, H2M 1Y8, Canada.

Email: brahim.brahmi@collegeahuntsic.qc.ca

Present address

Department of Electrical engineering, College Ahuntsic, Montreal, Quebec, H2M 1Y8, Canada.

Funding information

The authors declare that no funds, grants, or other support were received during the preparation of this manuscript

Abstract

This study addresses two issues about the interaction of the upper limb rehabilitation robot with individuals who have disabilities. The first step is to estimate the human's target position (also known as TPH). The second step is to develop a robust adaptive impedance control mechanism. A novel Non-singular Terminal Sliding Mode Control combined with an adaptive super-twisting controller is being developed to achieve this goal. This combination's purpose is to provide high reliability, continuous performance tracking of the system's trajectories. The proposed adaptive control strategy reduces matched dynamic uncertainty while also lowering chattering, which is the sliding mode's most glaring issue. The proposed TPH is coupled with adaptive impedance control with the use of a Radial Basis Function Neural Network, which allows a robotic exoskeleton to simply track the desired impedance model. To validate the approach in real-time, an exoskeleton robot was deployed in controlled experimental circumstances. A comparison study has been set up to show how the adaptive impedance approach proposed is better than other traditional controllers.

KEYWORDS

adaptive control, impedance model, robust control, super twisting controller, upper limb rehabilitation robot

1 | INTRODUCTION

Several medical conditions can cause limited mobility. Spasticity, relaxation and involuntary muscle contractions are examples of these. Meanwhile, more chronic cases are frequently caused by sensory paralysis due to a variety of causes, including cerebral palsy, stroke, muscular dystrophy or polio syndrome [1]. Aging is also frequently associated with decreased mobility [1]. This places a strain on their families, communities and the country as a whole. According to the authors in Ref. [2], rehabilitation programs are the most effective method for encouraging functional recovery in these patients. Traditional rehabilitation necessitates a lengthy commitment from a therapist or doctor [2]. Unfortunately, qualified therapists are in short supply. In addition, therapy usually takes a very long time and requires the therapist to spend many hours with each

patient. Extensive research has been conducted in several disciplines of robotics, particularly on wearable robots, such as exoskeleton robots [3–7]. A rehabilitation robot can be used to provide various passive, active, active-assisted and virtual rehabilitation therapies to patients undergoing upper limb rehabilitation. A robotic rehabilitation system can perform repetitive therapy treatments without tiring or limiting the patient's dosage [8, 9].

Patients in the “active rehabilitation therapy” mode practice a variety of functional activities (e.g., grasping and reaching movements) and receive occasional visual and haptic input (e.g., visual feedback and haptic feedback) [8]. The patient's ability to perform daily tasks on his or her own can be evaluated and encouraged through the use of active-assisted rehabilitative motion. Some robotics solutions are cumbersome and bulky, making them incapable of providing guided or

Abbreviations: ABC, a black cat; DEF, doesn't ever fret; GHI, goes home immediately.

Brahim Brahmi, Mohammad Habibur Rahman and Maarouf Saad contributed equally to this study.

This is an open access article under the terms of the Creative Commons Attribution-NonCommercial-NoDerivs License, which permits use and distribution in any medium, provided the original work is properly cited, the use is non-commercial and no modifications or adaptations are made.

© 2023 The Authors. *IET Cyber-Systems and Robotics* published by John Wiley & Sons Ltd on behalf of Zhejiang University Press.

active rehabilitation therapy. Rehabilitation and assisting robots' user-friendliness depended heavily on compliance control [10]. The patient's force can be accommodated by the aided robot through compliance control. Exoskeleton robots are capable of tracking the wearer's movement in this scenario, allowing for human-exoskeleton cooperation [11]. In compliance control for rehabilitation robots, one of the most difficult issues is predicting the specific human's planned motion so that the exoskeleton robot does not become a load when the patient desires to change motion. By using Neural Networks (NNs), several studies have attempted to forecast human's target position (TPH) [12–15]. The following are the most common drawbacks of these approaches: (1) The training procedure must be restarted if the human's purpose changes throughout the run time; (2) During the training process, TPH is required, which might be challenging to acquire in real-time; and (3) the NN has to be taught to each patient before beginning. Even when a person modifies their intended motion, TPH remains accurate because of an updated law proposed in this research. Furthermore, there is no requirement for the real TPH in the proposed solution. This study presents an updated law to online tweak the NN weights, allowing TPH accuracy to be maintained despite alterations in human-intended movements. Furthermore, the exact TPH is not required for the proposed approach.

Control strategies for uncertain non-linear systems (Euler-Lagrange (EL) systems) have traditionally employed adaptive and resilient control procedures [16, 17]. Costly calculations of system parameters and controller gains are required for adaptive control, but not for robust control [18]. Strong control is nevertheless constrained by the need to set the uncertainty bound in advance. The switching law advantages are overstated if not correctly defined, as is the case with sliding mode control (SMC) [19] and robust outer-loop control [20]. This causes unwanted chattering and a loss of control accuracy [21], which has led researchers to examine the benefits of combining the two techniques into an adaptive-robust control method.

Subsequently, several finite-time control strategies, such as terminal SMC (TSMC) [22, 23], have been developed to limit the occurrence of chattering. Although TSMC permits the achievement of finite-time control, it still presents a slow convergence speed and singularity issue. As a solution, fast TSMC (FTSMC) [24, 25] and non-singular TSMC (NTSMC) [26] have been conceived and investigated. These techniques, FTSMC and NTSMC, have effectively resolved the problem of fast finite-time convergence, but they have failed to address the singularity issue. Consequently, non-singular FTSMC has been developed as a method that satisfies both requirements [27, 28]. The integral SMC (ISMC) [29] and the proportional-integral-derivative SMC [30] both had the ability to improve the SMC's transient responsiveness as well. Integral TSMC [31, 32], on the other hand, was designed based on both ISMC and TSMC to achieve both quick transient response and finite-time convergence. All of the previously described control systems are, however, interconnected or strongly based on more traditional control approaches, and this should be noted. As a result, all of

SMC's previously identified flaws persist, leading to the current state of the art.

Recent studies have led to the development of a second-order control known as super twisting [33]. This controller is one of the most efficient algorithms, according to the authors in Ref. [34]. In addition, super twisting ensures that the sliding surface and its derivative will converge to zero in finite time in a theoretically precise manner. However, from the perspective of chattering, the twisting controller is the worst option because the profits must be at least twice as large as the upper limit of uncertainties. In addition, the amplitude of chattering produced by the twisting controller is greater than the amplitude of chattering produced by the linear sliding surface relay controller. In addition, the upper-bound uncertainties are not always accessible in real-time, particularly when rapid dynamic motion is present.

Motivated by the challenges raised above, this work suggests a unique control method to address two issues concerning the upper limb rehabilitation robot's collaboration with impaired individuals. (1) Estimation of the exoskeleton's wearer's TPH. (2) Robust adaptive impedance control to ensure joint position state convergence to the TPH. A Radial Basis Function Neural Network (RBFNN) was created to tune online and deliver an accurate estimation of the subject's TPH. As the rest position of a desired target impedance mode, the expected intended motion is merged into the created impedance control. Then, adaptive super twisting with strong adaptive impedance control is devised. However, because the top bound value of the matched uncertainties can be established in advance, the gains of the twisting controller should be at least twice as large as the upper bound value of the uncertainties, which generates chattering. To address this issue, a novel Non-singular Terminal Sliding Mode surface (NTSMS) was created, specifically to address the singularity problem and significantly improve transient performance. Following that, finite-time stability analysis for NTSMS was performed, demonstrating the system's stability. Second, an updated law control is intended to modify the upper bound of the uncertainties, allowing them to be rejected while reducing unwanted chattering. Finally, the experimental results from test cases performed with an exoskeleton robot supported the suggested control scheme's higher real-time performance. The following are the key contributions investigated in this study:

- Based on the patient's exerted force, an intelligent approach is given to forecast the desired TPH.
- A human-robot collaboration impedance model is constructed. The estimated desired motion has been included in the impedance control of the exoskeleton robot, causing it to actively pursue its wearer.
- To achieve finite-time convergence, fast transient response, minimal chattering and prevent singularity, an adaptive super-twisting control based on a novel non-singular terminal sliding mode surface was developed.
- The updated law was created to account for unknown dynamics. Prior knowledge of the upper bounds of particular unknown system parameters was not required in advance,

allowing the super-twisting approach to overcome its well-known limitation.

- Experiments were carried out to assess the suggested control scheme's performance in terms of providing a quick transient response, a minimal steady-state error and minimised chattering.

This paper's remainder is structured as follows: In Section 2, the overview and problem description are provided. In Section 3, the estimated TPH based on machine learning is shown. Section 4 details the novel sliding surface and adaptive super twisting with its stability analysis. In Section 5, the assisted exoskeleton robot is illustrated. Experimental results and comparative study are shown in Section 6. Finally, conclusions and potential future work are discussed in Section 7.

2 | PRELIMINARIES AND PROBLEM FORMULATION

2.1 | Problem formulation

The dynamic behaviour of the exoskeleton robot with n -DOFs can be characterised as follows:

$$M(q)\ddot{q} + Z(q, \dot{q}) = \tau - J^T(q)f(t) \quad (1)$$

with

$$\eta = \zeta(q); \quad \dot{\eta} = J(q)\dot{q}; \quad \ddot{\eta} = J(q)\ddot{q} + \dot{J}(q)\dot{q} \quad (2)$$

where $q \in \mathbb{R}^n$ is the joint position of the robotic exoskeleton, while $\eta \in \mathbb{R}^n$ is its Cartesian position. $M(q) \in \mathbb{R}^{n \times n}$ is the inertia matrix, $Z(q, \dot{q}) = C(q, \dot{q})\dot{q} + G(q)$ with $C(q, \dot{q}) \in \mathbb{R}^{n \times n}$ is the centripetal and Coriolis term and the gravitational term of the robotic exoskeleton, respectively, $J(q) \in \mathbb{R}^{n \times n}$ is the Jacobian matrix of the exoskeleton, and $\zeta(q)$ is the direct kinetics of the robotic exoskeleton. $f(t) \in \mathbb{R}^n$ represents the interaction forces, and $\tau \in \mathbb{R}^n$ is the torque input.

Using impedance control, the exoskeleton is instructed to be flexible in response to the wearer's force. The base impedance model dominates the dynamic of the robotic exoskeleton by the following equation:

$$M_d(\ddot{\eta} - \ddot{\eta}_d) + C_d(\dot{\eta} - \dot{\eta}_d) + G_d(\eta - \eta_d) = f(t) \quad (3)$$

where η is the Cartesian measured position of the robotic exoskeleton, and η_d is its Cartesian rest position. M_d , C_d and G_d are the intended inertia, damping and stiffness matrices, respectively.

In Equation (3), the exoskeleton robot's location η is governed by the interaction force $f(t)$. From the patient's perspective, it is similar to transferring an object with inertial/mass M_d , damping C_d and stiffness G_d from η_d to η . If η_d and η

differ greatly, the patient needs more strength to move the robotic exoskeleton. If the exoskeleton “knows” the wearer's intended motion and adjusts η_d accordingly, the patient will use less force.

2.2 | Preliminaries

The equation (Equation 1) can be rewritten due to unknown dynamics, load variations and uncertain parameters as follows:

$$M_K(q)\ddot{q} + Z_K(q, \dot{q}) + \Pi(q, \dot{q}, \ddot{q}) = \tau - J^T(q)f(t) \quad (4)$$

where $\Pi(q, \dot{q}, \ddot{q})$ is referred to as follows:

$$\Pi(q, \dot{q}, \ddot{q}) = M_U(q)\ddot{q} + Z_U(q, \dot{q}) \quad (5)$$

where \bullet_K represents the known term of \bullet while \bullet_U is the part that is uncertain. It is possible to rearrange the dynamic model in (Equation 4) as follows:

$$\ddot{q} = N(q, \dot{q}) + g(q)\tau + U \quad (6)$$

where $N(q, \dot{q}) = -M_K^{-1}(q)(Z_K(q, \dot{q}) + J^T(q)f(t))$ is the non-linear dynamic vector that is well-known, $U = -M_K^{-1}(q)\Pi(q, \dot{q}, \ddot{q})$ is the bounded matched uncertainty and $g(q) = M_K^{-1}(q)$ is the control matrix.

The primary purposes of this study are to design an impedance-adaptive super-twisting control strategy that guarantees: 1) The estimation of the subject's target position q_d based on a smart approach, 2) The robotic exoskeleton expressed in Equation (1) can follow the generated trajectory with high accuracy, even in the presence of matched dynamic uncertainty and 3) A fast transient response and finite-time convergence of the dynamical system of robotic exoskeleton. In this regard, the following lemma and assumption are deemed verified in the subsequent section:

Assumption 1 The matched uncertain function U_i for $i = 1, \dots, n$ are bounded:

$$|U_i| \leq \Omega_i$$

where $\Omega_i > 0$ for $i = 1, \dots, n$.

Lemma 1 [35] For any constants $c_1 > 0$ and $0 < c_2 < 1$, an extended Lyapunov condition of finite-time stability can be given in the form of a fast terminal sliding mode as follows:

$$\dot{V} + \sum_{i=1}^n c_1 V^{c_2} \leq 0$$

where the settling time can be estimated by:

$$T_s \leq \frac{V^{1-c_2}(e_0)}{c_1(1-c_2)}$$

with $V(x_0)$ being the initial value of the Lyapunov function.

3 | ASSIMILATION OF THE TPH VIA RBFNNS APPROACH

The damper and spring elements are widely used to regulate the impedance model, as discussed in Ref. [15]. The impedance model (Equation 3) can thus be reduced to the following equation:

$$C_d \dot{\eta} + G_d(\eta_d - \eta) = f(t) \quad (7)$$

Consider the fact that the parameters C_d and G_d are not linear and change when the user's upper limb position varies in the dynamic model (Equation 6). The TPH, on the other hand, may be derived using the force produced by the user during the interaction between the exoskeleton and the user, the real position η , and its derivative $\dot{\eta}$ as follows:

$$\Delta\eta_d = F(\dot{\eta}, \eta, f) = F(z) \quad (8)$$

In order to arrive at the following prediction for TPH (q_d):

$$q_{d(k+1)} = q_{d(k)} + \zeta^{-1}(\Delta\eta_d) \quad (9)$$

where $\zeta^{-1}(\Delta\eta_d)$ is the exoskeleton inverse kinematics solution. The actual discrete position is represented by $q_{d(k)}$, and the next discrete value is represented by $q_{d(k+1)}$. The user's target position can be predicted if $\Delta\eta_d$ is approximated in this case. RBFNNS are employed to achieve this goal. The RBFNN framework is depicted as follows [36]:

$$\begin{aligned} \Delta\eta_d &= F(z) = W^T \Phi(z) \\ \Phi(z) &= [\phi_1(z), \phi_2(z), \dots, \phi_l(z)]^T \\ \phi_i(z) &= \exp\left[-\frac{(z - \rho_i)^T (z - \rho_i)}{\pi_i^2}\right] \\ i &= 1, 2, \dots, l \end{aligned} \quad (10)$$

where, $z = [f^T, \eta^T, \dot{\eta}^T]^T \in \mathbb{R}^m$ represents the input of RBFNN, $W = [w_1, w_2, \dots, w_l]^T \in \mathbb{R}^{l \times m}$, $l > 1$ is NN nodes number, $w_i \in \mathbb{R}^m$. W represents the ideal weight vector. ρ_i is the centre of the receptive field and π_i is the width of the Gaussian function.

According to the outputs of RBFNN, the TPH can be updated as follows:

$$\Delta\eta_d = \hat{W}^T \Phi(z) + \varpi \quad (11)$$

where ϖ represents the estimation error, \hat{W} represents the estimate of the ideal weight W , and Φ has the identical definition as that determined in Equation (10). It is known that ϖ can be made artificially small, if l is adequately high.

Moreover, $\Phi_i(z)$ is achieved by collecting z data, which are actual position, velocity and forces of the subject and \hat{W} is collected by applying a back propagation algorithm [37] in Equation (11). The goal is to have the exoskeleton robot "actively" push towards the user's target position, hence minimising the interaction force f . Therefore, \hat{W} is updated in the direction of the steepest descent relative to the cost function, so

$$T_i = \frac{1}{2} f_i^2 \quad (12)$$

Hence,

$$\begin{aligned} \dot{\hat{W}}_i &= -a' \frac{\partial T_i}{\partial \hat{W}_i} \\ &= -a' \frac{\partial T_i}{\partial f_i} \frac{\partial f_i}{\partial \eta_{di}} \frac{\partial \eta_{di}}{\partial \hat{W}_i} \\ &= -a' f_i \frac{\partial f_i}{\partial \eta_{di}} \frac{\partial \eta_{di}}{\partial \hat{W}_i} \end{aligned} \quad (13)$$

where $a' > 0$, the term $\frac{\partial f_i}{\partial \eta_{di}}$ can be obtained from Equation (7) as follows:

$$\frac{\partial f_i}{\partial \eta_{di}} = G_{di} \quad (14)$$

and $\frac{\partial \eta_{di}}{\partial \hat{W}_i}$ can be obtained from Equation (11) as follows:

$$\frac{\partial \eta_{di}}{\partial \hat{W}_i} = \Phi_i(z) \quad (15)$$

Combining Equation (14) and Equation (15) into Equation (13) is as follows:

$$\dot{\hat{W}}_i = -a f_i \Phi_i(z) \quad (16)$$

where $a = a' G_{di}$, while G_{di} is an unknown parameter, it can be absorbed by a .

4 | CONTROL DESIGN AND STABILITY ANALYSIS

Tracking error $e = q - q_d$ is defined as the difference between the actual position q and q_d provided by Equation (9), which is regarded to be TPH. The proposed surface is designed as follows to achieve a fast transient response and finite-time convergence without any singularity problem:

$$\sigma = e + \lambda_1 |\dot{e}|^\beta \text{sign}(\dot{e}) \quad (17)$$

where $\lambda_1 > 0$ is the positive constant, $|\dot{e}|^\beta = \text{diag}(|\dot{e}_1|^\beta, \dots, |\dot{e}_n|^\beta)$ with $1 < \beta < 2$.

Theorem 1 *The suggested sliding surface (Eq.17) is capable of achieving a stable and rapid response to finite-time convergence. Moving from $e(T_r) \neq 0$ to $e(T_r + T_s) = 0$ takes a finite time T_s that is denoted by*

$$T_s \leq \frac{V^{1-\mu}(\dot{e}_0)}{v(1-\mu)}$$

where $v = \left(\frac{1}{\lambda_1}\right)^{\frac{1+\beta}{\beta}} 2^{\frac{1+\beta}{2\beta}}$ and $\mu = \frac{1+\beta}{2\beta}$ with the starting state of the Lyapunov function being $V(e_0)$.

Proof: See Appendix A.

4.1 | Design of robust super-twisting control based on non-singular fast terminal sliding mode surface

The first derivative of the designed sliding surface (Equation 17) can be determined as follows:

$$\dot{\sigma} = \dot{e} + \psi(\dot{e})\ddot{e} = \dot{e} + \psi(\dot{e})[N(q, \dot{q}) + g(q)\tau + U - \ddot{q}_d] \quad (18)$$

where $\psi(\dot{e}) = \beta\lambda_1 |\dot{e}|^{\beta-1}$. The following is the definition of the chosen Lyapunov function:

$$V_1 = \frac{1}{2}\sigma^T \sigma \quad (19)$$

Differentiating V_1 by using Equation (18) gives the following equation:

$$\begin{aligned} \dot{V}_1 &= \sigma^T \dot{\sigma} \\ &= \sigma^T [\dot{e} + \psi(\dot{e})(N(q, \dot{q}) + g(q)\tau + U - \ddot{q}_d)] \end{aligned} \quad (20)$$

The closed-loop of the system based on super-twisting control can be given as follows:

$$\begin{aligned} \dot{e} + \psi(\dot{e})[N(q, \dot{q}) + g(q)\tau + U - \ddot{q}_d] &= -\lambda_2 \sigma \\ -K_1 \Lambda(\sigma) \text{sign}(\sigma) - K_2 \int_0^t \text{sign}(\sigma) dt & \end{aligned} \quad (21)$$

where $\Lambda(\sigma) = \text{diag}(|\sigma_1|^{0.5}, \dots, |\sigma_n|^{0.5})$, $K_1 \in \mathbb{R}^{n \times n}$ and $\lambda_{\min}(K_1) > 0$, $K_2 \in \mathbb{R}^{n \times n}$ and $\lambda_{\min}(K_2) > 0$, $\lambda_2 \in \mathbb{R}^{n \times n}$ and $\lambda_{\min}(\lambda_2) > 0$, and $\text{sign}(\sigma) = [\text{sign}(\sigma_1), \dots, \text{sign}(\sigma_n)]^T$ is determined such that

$$\text{sign}(\sigma_i) = \begin{cases} 1, & \text{if } \sigma_i > 0 \\ 0, & \text{if } \sigma_i = 0 \\ -1, & \text{if } \sigma_i < 0 \end{cases} \quad (22)$$

Then, resolving (Equation 21), the proposed robust super-twisting control based on non-singular terminal sliding mode control is designed as follows:

$$\tau = \psi(\dot{e})^{-1} g(q)^{-1} (u_n - u_\sigma) \quad (23)$$

where

$$u_n = -\psi(\dot{e})(N(q, \dot{q}) - \ddot{q}_d) - \dot{e} \quad (24)$$

and

$$u_\sigma = \lambda_2 \sigma + K_1 \Lambda(\sigma) \text{sign}(\sigma) + K_2 \int_0^t \text{sign}(\sigma) dt \quad (25)$$

where $\psi(\dot{e})^{-1} = \frac{1}{\beta\lambda_1} |\dot{e}|^{2-\beta}$. Substituting the torque input (23) in \dot{V}_1 (20) yields

$$\begin{aligned} \dot{V}_1 &= \sigma^T (\psi(\dot{e})U - \lambda_2 \sigma) \\ &+ \sigma^T \left(-K_1 \Lambda(\sigma) \text{sign}(\sigma) - K_2 \int_0^t \text{sign}(\sigma) dt \right) \\ &= \sum_{i=1}^n -\lambda_{2i} \sigma_i^2 - K_{1i} |\sigma_i|^{1.5} \\ &- \sum_{i=1}^n -\sigma_i \psi_i(\dot{e}_i) U_i + K_{2i} \sigma_i \int_0^t \text{sign}(\sigma_i) \end{aligned} \quad (26)$$

Based on **Assumption 1**, assuming that U_i is a bounded smooth known function that can be expressed as follows:

$$\Omega_i = \chi \psi(\dot{e})^{-1} |\sigma_i|^{0.5} \quad (27)$$

where χ is a positive constant. In the case where $\sigma_i > 0$ and $\text{sign}(\sigma_i) = 1$, \dot{V}_1 (Equation 26) becomes

$$\begin{aligned} \dot{V}_1 &= -\sum_{i=1}^n |\sigma_i| (\lambda_{2i} |\sigma_i| + K_{1i} |\sigma_i|^{0.5} - \psi_i(\dot{e}_i) U_i + K_{2i} t) \\ &\leq \sum_{i=1}^n -\lambda_{2i} \sigma_i^2 + |\sigma_i|^{1.5} (\chi - K_{1i}) - K_{2i} |\sigma_i| t \end{aligned} \quad (28)$$

To ensure that (Equation 28) is negative semi-definite, it is required to achieve the following sufficient condition:

$$\chi \leq K_{1i} \quad (29)$$

When $\sigma_i < 0$ and $\text{sign}(\sigma_i) = -1$, \dot{V}_1 (Equation 26) becomes

$$\begin{aligned} \dot{V}_1 &= -\sum_{i=1}^n |\sigma_i| (\lambda_{2i} |\sigma_i| + K_{1i} |\sigma_i|^{0.5} - \psi_i(\dot{e}_i) U_i + K_{2i} t) \\ &\leq \sum_{i=1}^n -\lambda_{2i} \sigma_i^2 + |\sigma_i|^{1.5} (\chi - K_{1i}) - K_{2i} |\sigma_i| t \end{aligned} \quad (30)$$

As a result, \dot{V}_1 is negative semi-definite if the condition in (Equation 29) is satisfied. The closed-loop system's stability is thus demonstrated.

4.2 | Design adaptive robust super-twisting control based on non-singular fast terminal sliding mode surface

In real-time, it is difficult to estimate the bound value of matched uncertainty in advance. As proposed in the Equations (23)–(25), it is assumed that the upper bound value of the unknown function Ω could be obtained in advance. An adaptive law is designed in this section to resolve this issue as follows:

$$\tau = \psi(\dot{e})^{-1} g(q)^{-1} (u_{an} - u_\sigma) \quad (31)$$

where u_σ is proposed just similar to in Equation (25), and the adaptive law can be re-designed as

$$u_{an} = -\psi(\dot{e}) (N(q, \dot{q}) + \hat{\Omega} - \dot{q}_d) - \dot{e} \quad (32)$$

where $\hat{\Omega}$ is employed to estimate the matched uncertainty U . It is approximated by utilising the updated law:

$$\dot{\hat{\Omega}} = \frac{1}{\varepsilon} \psi(\dot{e}) |\sigma| \quad (33)$$

where ε is a positive constant. It is worth mentioning that the above law will always fulfil **Assumption 1**. Let $\tilde{\Omega} = \hat{\Omega} - \Omega$ be the estimation error. The following Lyapunov function is as follows:

$$V_2 = V_1 + \frac{1}{2} \varepsilon \tilde{\Omega}^T \tilde{\Omega} \quad (34)$$

The derivative of the Lyapunov function (34) can be acquired as follows:

$$\begin{aligned} \dot{V}_2 &= \dot{V}_1 + \varepsilon \tilde{\Omega}^T \dot{\tilde{\Omega}} \\ &= \sigma^T \psi(\dot{e}) U - \sigma^T \psi(\dot{e}) \hat{\Omega} - \sigma^T \lambda_2 \sigma + \tilde{\Omega}^T \psi(\dot{e}) \sigma \\ &\quad + \sigma^T \left(-K_1 \Lambda(\sigma) \text{sign}(\sigma) - K_2 \int_0^t \text{sign}(\sigma) dt \right) \end{aligned} \quad (35)$$

Utilising **Assumption 1**, the Equation (35) further yields

$$\begin{aligned} \dot{V}_2 &\leq -\sigma^T \psi(\dot{e}) \tilde{\Omega} - \sigma^T \lambda_2 \sigma + \tilde{\Omega}^T \psi(\dot{e}) |\sigma| \\ &\quad + \sigma^T \left(-K_1 \Lambda(\sigma) \text{sign}(\sigma) - K_2 \int_0^t \text{sign}(\sigma) dt \right) \\ &= \sum_{i=1}^n -\lambda_{2i} \sigma_i^2 - K_{1i} |\sigma_i|^{1.5} - \sigma_i \psi_i(\dot{e}_i) \tilde{\Omega}_i \\ &\quad - \sum_{i=1}^n -|\sigma_i| \psi_i(\dot{e}_i) \tilde{\Omega}_i + K_{2i} \sigma_i \int_0^t \text{sign}(\sigma_i) \end{aligned} \quad (36)$$

When $\sigma_i > 0$ and $\text{sign}(\sigma_i) = 1$, \dot{V}_2 (Equation 36) becomes

$$\begin{aligned} \dot{V}_2 &= -\sum_{i=1}^n |\sigma_i| (\lambda_{2i} |\sigma_i| + K_{1i} |\sigma_i|^{0.5} + \psi_i(\dot{e}_i) \tilde{\Omega}_i - \psi_i(\dot{e}_i) \tilde{\Omega}_i \\ &\quad + K_{2i} t) \\ &\leq \sum_{i=1}^n -\lambda_{2i} \sigma_i^2 - K_{1i} |\sigma_i|^{1.5} - K_{2i} |\sigma_i| t \end{aligned} \quad (37)$$

It is clear that Equation (37) is negative semi-definite. In the case where $\sigma_i < 0$ and $\text{sign}(\sigma_i) = -1$, \dot{V}_2 (Equation 36) becomes

$$\begin{aligned} \dot{V}_2 &= -\sum_{i=1}^n |\sigma_i| (\lambda_{2i} |\sigma_i| + K_{1i} |\sigma_i|^{0.5} + \psi_i(\dot{e}_i) \tilde{\Omega}_i - \psi_i(\dot{e}_i) \tilde{\Omega}_i \\ &\quad + K_{2i} t) \\ &\leq \sum_{i=1}^n -\lambda_{2i} \sigma_i^2 - K_{1i} |\sigma_i|^{1.5} - K_{2i} |\sigma_i| t \end{aligned} \quad (38)$$

Consequently, \dot{V}_2 is negative semi-definite without the satisfying condition in Equation (29). Hence, the closed-loop system stability is proven. The scheme of the proposed approach is illustrated in Figure 1.

5 | ROBOTIC EXOSKELETON DEVELOPMENT

Rehabilitation robots have human-like anatomy so that they can improve and rehabilitate human upper limb mobility. Humans may wear a MARSE robot that moves in unison with their own body movements. Furthermore, MARSE's design was derived from human arm anatomy and designed to be suitable for exoskeleton users partaking in physical and/or occupational therapy activities. The structure of the developed MARSE robot worn by a human is depicted in Figure 2 (human-robot interaction). The scapulohumeral (shoulder)

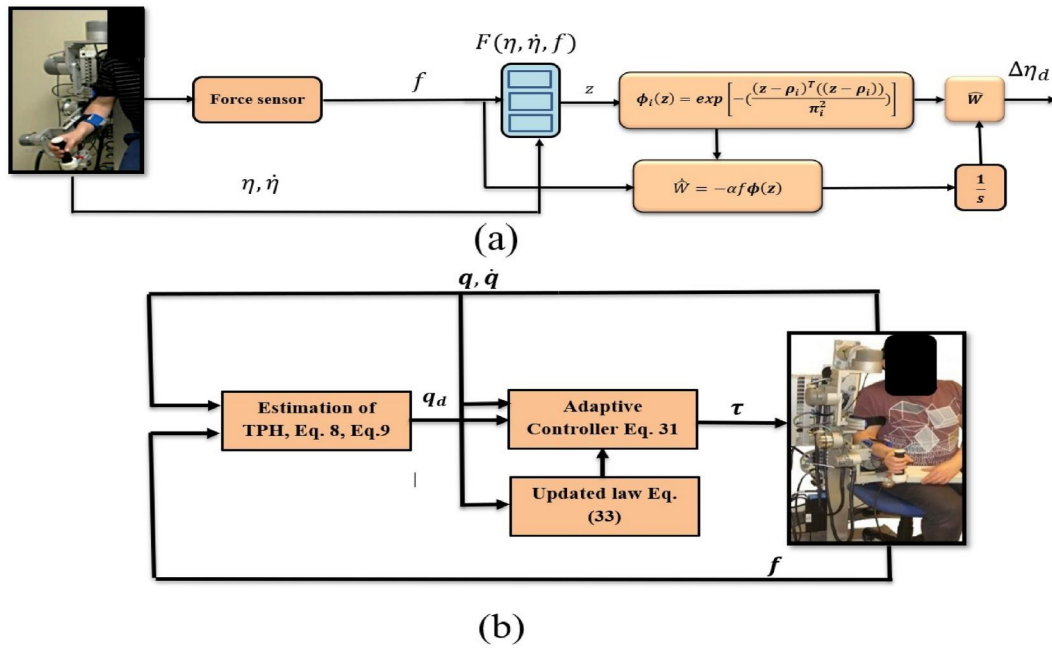


FIGURE 1 (a) The assimilation of TPH. (b) The suggested controller. TPH, human's target position

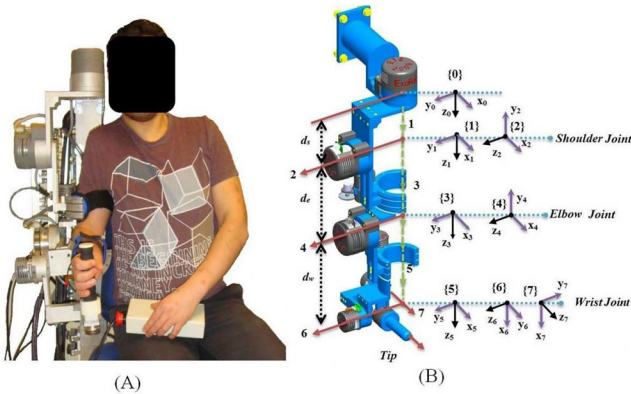


FIGURE 2 (a) The human-robot collaboration, (b) The exoskeleton reference frames (MARSE) [39]

joint is in charge of a number of upper limb movements. The first two joints are responsible for vertical and horizontal scapulohumeral extension/flexion movements, while the third joint is meant to rotate the shoulder inward and outward. A single joint is employed to complete the flexion/extension motion of the elbow in the elbow portion. The wrist is made up of three joints that make up the last part of the upper limb: The first joint is responsible for forearm pronation and supination, whereas the second and third joints are responsible for ulnar/radial deviation and flexion/extension movements, respectively. In comparison to other exoskeleton robots, the MARSE robot boasts a number of unique features, including the ability to be worn comfortably, a high power-to-weight ratio and a low weight. It can also correct for gravity as well as conduct a variety of upper limb movements. Our earlier published paper [38] can be helpful to newbie readers.

6 | EXPERIMENTS VERIFICATION AND COMPARATIVE EVALUATION

6.1 | Experiment description

On the MARSE exoskeleton robot, a real-time implementation was conducted to validate the control strategy. The real-time configuration consists of three treatment units, as depicted in Figure 3. The first is a desktop computer on which LabVIEW 2017 is used to construct the human-machine interface. The second consists of a National Instruments PXI unit with a sampling period of 500 μ s for the top-level control and 50 μ s for the low-level current control loop. Robotic exoskeleton joints are powered by brushless DC motors (Maxon EC-45 and Maxon EC-90) and integrated harmonic drives (gear ratios of 120:1 for motors one and two, whereas 100:1 for motors 3–7). The force sensor (RFT60-HA01 from Robotous Inc) is installed at the robot's very tip. In order to stimulate and evaluate the subject's performance, the MARSE robot is equipped with a Virtual Reality (VR) system that includes some function therapy exercises. Due to the mobility nature of the human's upper limb, the ethics commission has mandated that three distinct standards of safety be met at all times: First, a mechanical stopper that takes the subject's anatomical 7-DOFs into account; second, a software security level determined by torque control; and third, a manual security level determined by the user. As seen in Figure 3, the control system design is presented.

In order to experimentally evaluate the suggested controller (Equation 31) and TPH estimation (Equation 9) and (Equation 11), a healthy human subject wore the MARSE robot and was guided to perform the actively assisted activity. Using Equation (9), the resulting trajectory is updated online. In VR, geometric forms represent the active rehabilitation tasks that the

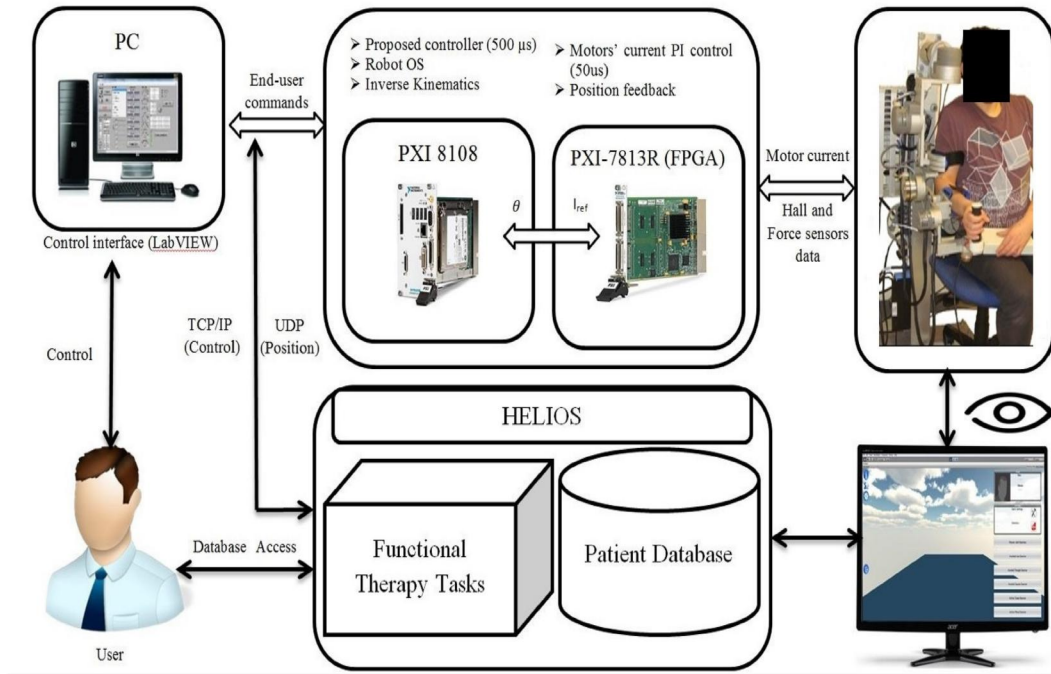


FIGURE 3 The Experimental platform

user must complete. The subject is asked to produce a force proportional to that of the virtual shape he is following from its origin to its destination in VR. Here, the subject performs all the tasks, while the exoskeleton robot only follows. In these test cases, a rectangle configuration was chosen. It is important to note that the pink colour in Figures 4 and 5 represents the patient's directed rectangle trajectory (Start position-Target 1-Target 2-Target 3- start position), in order to demonstrate that our algorithm respects the patient's desired motion intention (TPH). Joint angles were initially set to 0° for the MARSE, except for the elbow, which was set to 90° for all trials. The initial values of the control scheme were chosen as: $M_d = 0.01I_{6 \times 6}$, $C_d = 0.08I_{6 \times 6}$, $G_d = 0.001I_{6 \times 6}$ and $\chi = 0.1$. The number of NN nodes is $l = 10$, and the NN's parameters in (Equation 10) are $\rho_i = 0$ and $\pi_i = 1$ for $i = 1, 2, \dots, 10$. The adaptation ratio in (Equation 16) is $a = 0.01$. In the updating law, given by (Equation 33), parameters were set to be: $\varepsilon = 0.15$. The controller parameters were manually defined to be: $K_1 = 5.1I_{7 \times 7}$, $K_2 = 1.1I_{7 \times 7}$, $\beta = 1.5$, $\lambda_1 = 5.2$ and $\lambda_2 = 2.3$. It is worth mentioning that the MARSE robot was conducted by subject1 (age: 28 years; height: 168 cm; weight: 70 kg).

6.2 | Experimental results and analysis

The results of the experiments involving human-exoskeleton robot collaboration under the control law defined by (Equation 31), an estimation of the TPH (Equation 9) and (Equation 11) by using machine learning methods, RBFNNs, are shown in Figures 4, 6–8. In general, all of the findings demonstrated an efficient and smooth functioning, as shown in Figures 4, 6–8. The high Cartesian tracking performance of the

subject exoskeleton manipulator in VR is demonstrated in Figure 4. From this figure, it may deduce two important pieces of information: First, the TPH is quite accurate, which makes it possible to follow the lines of the rectangular in VR perfectly. Second, the suggested controller ensures that the exoskeleton robot swiftly follows the TPH of the subject. Figure 6 demonstrates that the suggested controller achieves a high level of performance with regard to joint tracking. This performance is achieved mostly as a result of the smoothness of the TPH when the machine learning operation is being performed (Equation 11).

At the same time, Figure 7 demonstrates quite plainly that the joint tracking errors decrease to levels close to zero in accordance with the control law (Equation 31), with a relatively high rate of convergence. Figure 8 displays an acceptable control input (τ) of the suggested method, which does not have an undesired chattering problem, with the exception of some chattering in joints six and seven. Therefore, the suggested control method exhibited good results despite the exoskeleton's dynamic model being subjected to unknown dynamics and online production of the reference trajectory. This was the case although the reference trajectory was generated online. As a result, the proposed control method produced satisfactory results.

6.3 | Comparative analysis

In the second scenario, The TPH of the subject: (age: 31 years; height: 170 cm; weight: 91 kg) is obtained by an optimisation approach [38] and was tracked using the conventional super-twisting controller [34]. The goal was to emphasise the

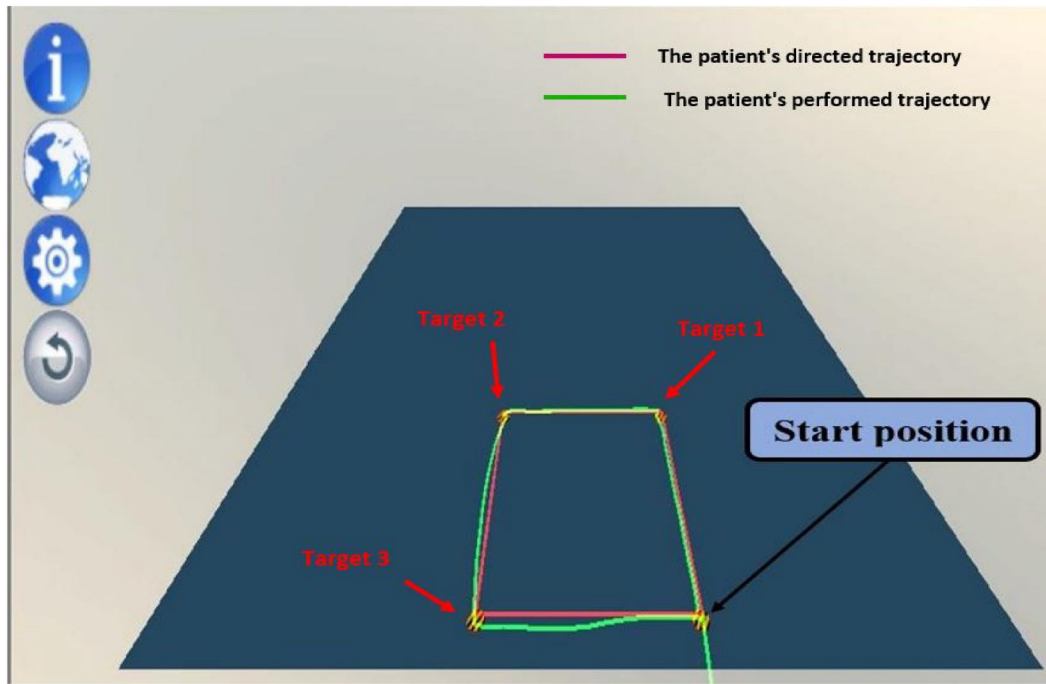


FIGURE 4 The Cartesian tracking performance of the human-exoskeleton robot in Virtual Reality (VR) under the proposed controller (Equation 31) and TPH estimation (Equation 9 and Equation 10). TPH, human's target position

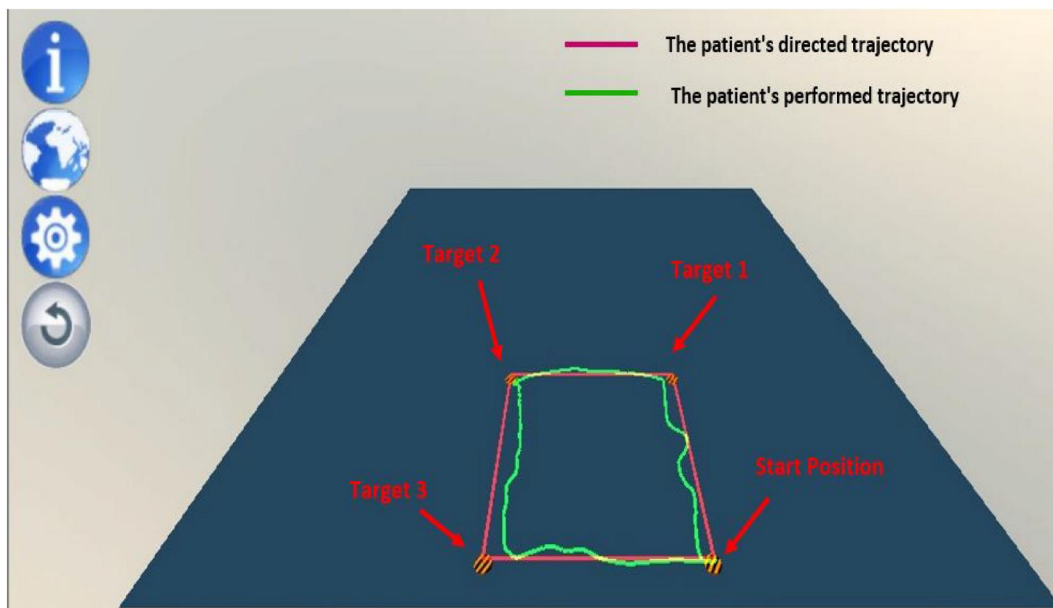


FIGURE 5 The performance of the human-exoskeleton robot's Cartesian tracking in VR using conventional approaches [34, 38]

benefits of the suggested adaptive impedance technique over other controllers.

The findings obtained using the conventional techniques [34, 38] were also satisfactory, as shown in Figures 5, 9–11. When Figures 4 and 5 are compared, it is clear that the estimation of TPH obtained through the learning strategy is superior to that obtained using the optimisation approach. The performance of the suggested controller in tracking the trajectory is shown in Figure 6, and it is superior to the performance

of the conventional technique shown in Figure 9. It is important to remark that the suggested control input in Figure 5 is significantly smoother than that of the conventional controller, in which there is unwelcome chattering, as illustrated in Figure 11, particularly in joints two, three, four and five. These findings provide conclusive evidence of the higher performance of the Impedance Learning Adaptive Super-Twisting Control strategy, which was proposed, in comparison to other conventional control approaches.

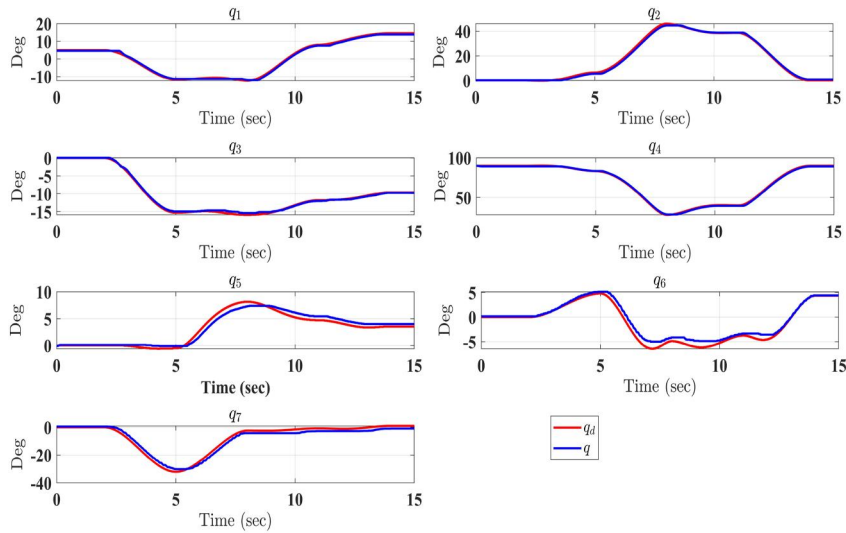


FIGURE 6 The joints tracking under the proposed controller (Equation 31) and TPH estimation (Equation 9 and Equation 10). TPH, human's target position

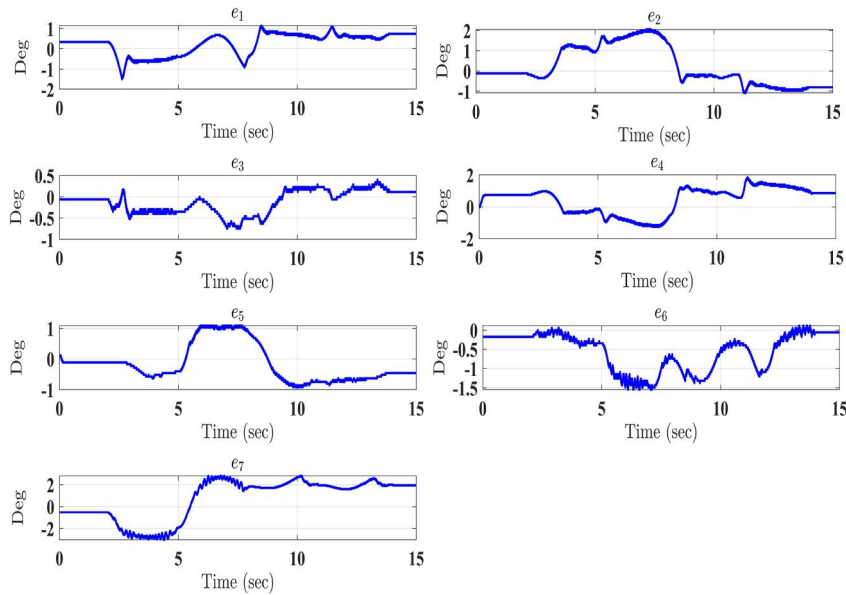


FIGURE 7 The joint tracking errors under the proposed controller (Equation 31) and TPH estimation (Equation 9 and Equation 10). TPH, human's target position

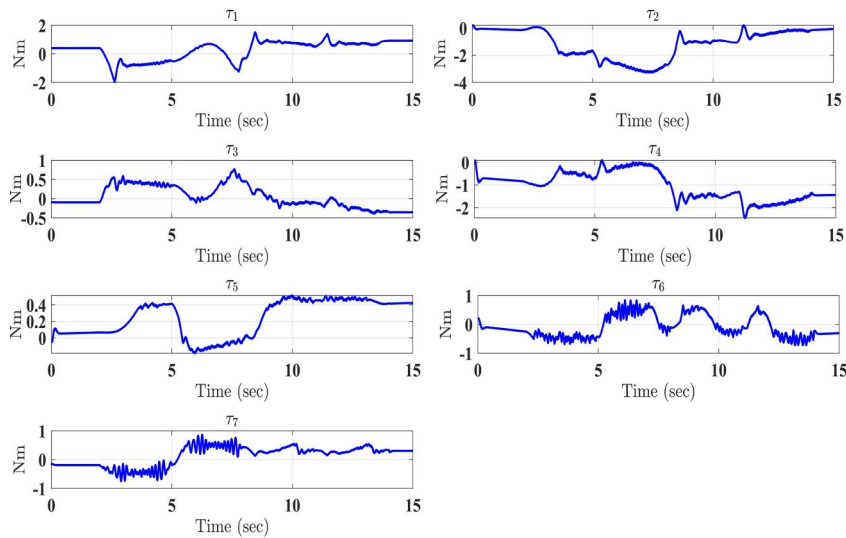


FIGURE 8 The generated torque inputs under the proposed controller (Equation 31) and TPH estimation (Equation 9 and Equation 10). TPH, human's target position

FIGURE 9 The joints tracking under conventional approaches [34, 38]

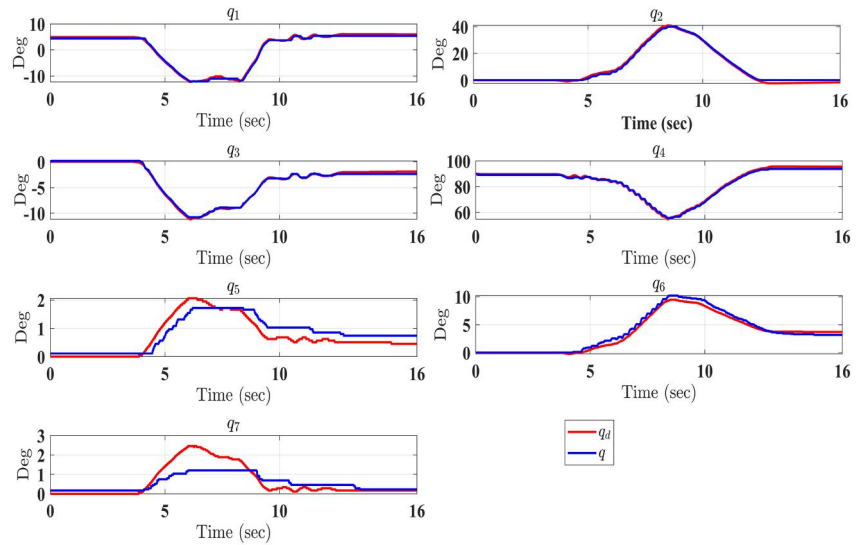


FIGURE 10 The joint tracking errors under conventional approaches [34, 38]

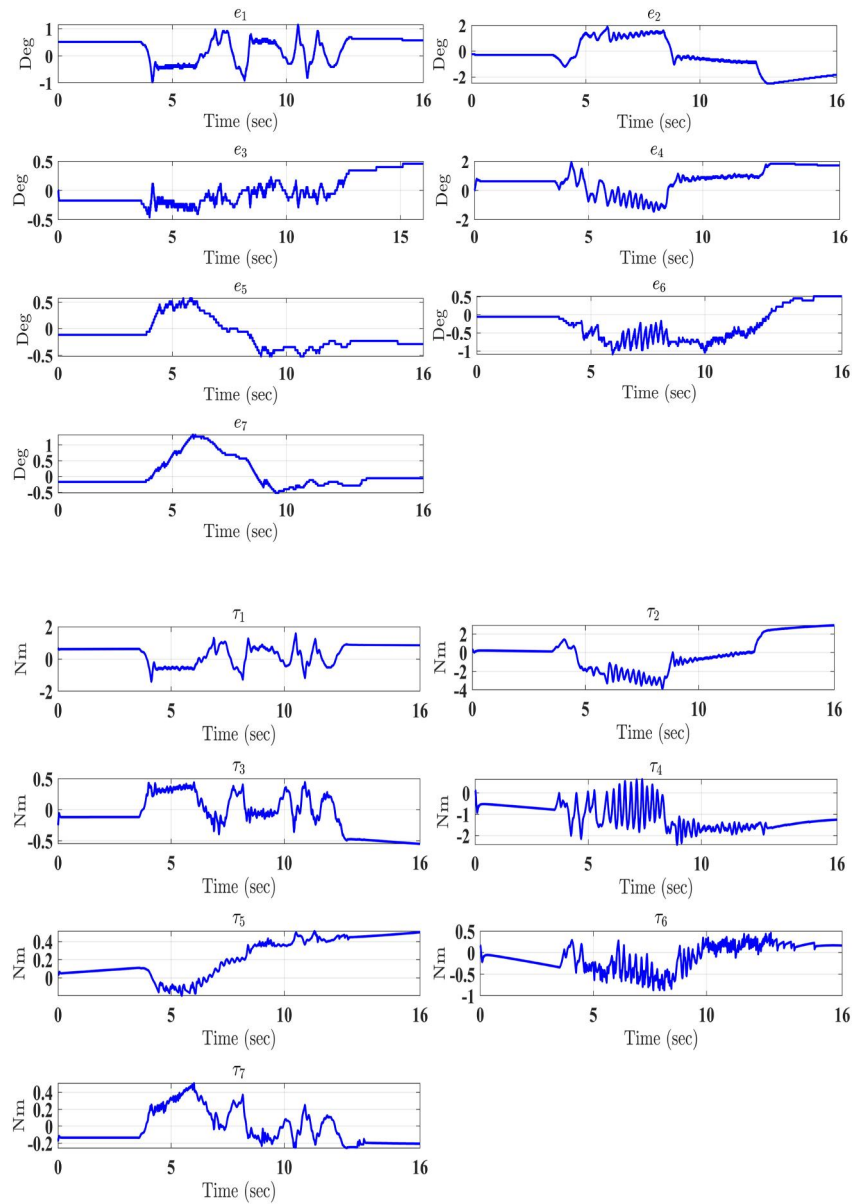


FIGURE 11 The generated torque inputs under conventional approaches [34, 38]

TABLE 1 Controllers performance

Regulator variables	Conventional controller [34, 38]	Proposed controller
RMS (e_1) (degrees)	2.10	1.392
RMS (e_2) (Degrees)	3.814	2.019
RMS (e_3) (Degrees)	1.987	1.511
RMS (e_4) (Degrees)	4.422	1.5074
RMS (e_5) (Degrees)	1.284	0.558
RMS (e_6) (Degrees)	0.922	0.5909
RMS (e_7) (Degrees)	1.564	2.0998
Execution time of TPH	1.25 ms	500 μ s

6.4 | Quantification of comparative study

Following the performance evaluation of the proposed approach scheme, a comparative quantification study was carried out to compare the performance of the intended control technique to conventional ones [34, 38]. The proposed RBFNNs algorithm was compared to an optimisation approach [38], both of which were used to estimate the subject's TPH. The proposed adaptive controller was then compared to the conventional control approach in another sensitivity analysis [34]. Table 1 summarises the Root Mean Square of joint errors and TPH algorithm execution time for each approach. It is evident that the proposed impedance controller consistently provided satisfactory tracking. This was the case despite the fact that the desired trajectory, TPH, was generated online, which could have negatively impacted the control system by causing a delay, and despite the fact that the exoskeleton's actual model dynamics were absent from the control law. While the conventional controller also produced acceptable results, its tracking error was significantly greater than that of the proposed controller. In addition, the TPH execution time provided by the RBFNN algorithm was significantly faster than that of the optimisation strategy [38]. This property summarises the effectiveness of combining the proposed controller with the RBFNN algorithm to generate an accurate trajectory in real-time. Consequently, the results confirmed the superior performance of the proposed controller in comparison to other conventional methods.

7 | CONCLUSIONS

In this article, two issues pertaining to human-exoskeleton robot collaboration were investigated. In each case, the TPH was approximated by making use of an impedance model and force feedback. The RBFNN is utilised in order to estimate the TPH, with the subject's force serving as the primary input. In order for the robotic exoskeleton to aggressively follow its wearer, the estimated TPH was set into the impedance control system and implemented in the exoskeleton. In order to provide finite-time convergence, fast transient response, less chattering and avoid singularity, a new adaptive impedance controller that is based on

super twisting and that is combined with a new novel NTSMC was designed. The matched dynamic uncertainties were automatically covered by an updated law. The well-known limitation of the super-twisting algorithm was successfully circumvented because it was not necessary, in advance, to have prior knowledge of the upper bounds of the individual uncertain system parameters. The TPH method has been verified, and the viability of the new controller has been tested, despite the fact that the exoskeleton's dynamic system is subject to matching uncertainties. Experimental results and a comparison study have been supplied. As part of future research, the impedance controller that was presented will be put through its paces on real-life stroke victims (individuals who have lost the motor function of their upper limb) to evaluate the robustness and precision of the proposed method.

CONFLICTS OF INTEREST

The authors declare that they have no conflict of interest.

DATA AVAILABILITY STATEMENT

The data that support the findings of this study are available from the corresponding author, Dr. Brahim Brahmi, upon reasonable request.

ORCID

Brahim Brahmi  <https://orcid.org/0000-0002-4486-0710>

REFERENCES

- Sidney, S., et al.: The heart disease and stroke statistics—2013 update and the need for a national cardiovascular surveillance system. *Am Heart Assoc* (2013)
- De Morand, A.: *Pratique de la rééducation neurologique*. Elsevier Masson (2014)
- Rahman, M.H., et al.: Development of a whole arm wearable robotic exoskeleton for rehabilitation and to assist upper limb movements. *Robotica* 33(1), 19–39 (2015). <https://doi.org/10.1017/s0263574714000034>
- Yu, S., et al.: Quasi-direct drive actuation for a lightweight hip exoskeleton with high backdrivability and high bandwidth. *IEEE ASME Trans. Mechatron.* 25(4), 1794–1802 (2020). <https://doi.org/10.1109/tmech.2020.2995134>
- Zhang, M., Davies, T.C., Xie, S.: Effectiveness of robot-assisted therapy on ankle rehabilitation—a systematic review. *J. NeuroEng. Rehabil.* 10(1), 30 (2013). <https://doi.org/10.1186/1743-0003-10-30>
- Liu, X., Wang, Q.: Real-time locomotion mode recognition and assistive torque control for unilateral knee exoskeleton on different terrains. *IEEE ASME Trans. Mechatron.* 25(6), 2722–2732 (2020). <https://doi.org/10.1109/tmech.2020.2990668>
- Teng, L., Gull, M.A., Bai, S.: PD-based fuzzy sliding mode control of a wheelchair exoskeleton robot. *IEEE ASME Trans. Mechatron.* 25(5), 2546–2555 (2020). <https://doi.org/10.1109/tmech.2020.2983520>
- Xie, S., et al.: Advanced robotics for medical rehabilitation. *Springer Tr. Adv. Robot.* 108, 1–41 (2016)
- Pinto-Fernandez, D., et al.: Performance evaluation of lower limb exoskeletons: a systematic review. *IEEE Trans. Neural Syst. Rehabil. Eng.* 28(7), 1573–1583 (2020). <https://doi.org/10.1109/tnsre.2020.2989481>
- Khan, A.M., et al.: Muscle circumference sensor and model reference-based adaptive impedance control for upper limb assist exoskeleton robot. *Adv. Robot.* 30(24), 1515–1529 (2016). <https://doi.org/10.1080/01691864.2016.1251335>
- Ao, D., Song, R., Gao, J.: Movement performance of human–robot cooperation control based on EMG-driven hill-type and proportional

- models for an ankle power-assist exoskeleton robot. *IEEE Trans. Neural Syst. Rehabil. Eng.* 25(8), 1125–1134 (2016). <https://doi.org/10.1109/tnsre.2016.2583464>
12. Lee, H.D., et al.: Human–robot cooperation control based on a dynamic model of an upper limb exoskeleton for human power amplification. *Mechatronics* 24(2), 168–176 (2014). <https://doi.org/10.1016/j.mechatronics.2014.01.007>
 13. Wakita, K., et al.: Human-walking-intention-based motion control of an omnidirectional-type cane robot. *IEEE/ASME Trans. Mechatronics* 18(1), 285–296 (2011). <https://doi.org/10.1109/tmech.2011.2169980>
 14. Chang, P.H., et al.: Stochastic estimation of human arm impedance using robots with nonlinear frictions: an experimental validation. *IEEE ASME Trans. Mechatron.* 18(2), 775–786 (2012). <https://doi.org/10.1109/tmech.2012.2184767>
 15. Rahman, M.M., Ikeura, R., Mizutani, K.: Investigation of the impedance characteristic of human arm for development of robots to cooperate with humans. *JSME Int. J. Series C Mechanical Systems, Machine Elements and Manufacturing* 45(2), 510–518 (2002). <https://doi.org/10.1299/jsmec.45.510>
 16. Plestan, F., et al.: New methodologies for adaptive sliding mode control. *Int. J. Control* 83(9), 1907–1919 (2010). <https://doi.org/10.1080/00207179.2010.501385>
 17. Liu, X., et al.: Adaptive robust control of a class of uncertain nonlinear systems with unknown sinusoidal disturbances. In: 2008 47th IEEE Conference on Decision and Control IEEE, pp. 2594–2599 (2008)
 18. Corless, M., Leitmann, G.: Continuous state feedback guaranteeing uniform ultimate boundedness for uncertain dynamic systems. *IEEE Trans. Automat. Control* 26(5), 1139–1144 (1981). <https://doi.org/10.1109/tac.1981.11102785>
 19. Slotine, J.J.E., Li, W.: *Applied Nonlinear Control*, vol. 199. Prentice hall, Englewood (1991)
 20. Khalil, H.K., Grizzle, J.W.: *Nonlinear Systems*, vol. 3. Prentice hall, Upper Saddle River (2002)
 21. Lee, H., Utkin, V.I.: Chattering suppression methods in sliding mode control systems. *Annu. Rev. Control* 31(2), 179–188 (2007). <https://doi.org/10.1016/j.arcontrol.2007.08.001>
 22. Wang, H., et al.: Design and implementation of adaptive terminal sliding-mode control on a steer-by-wire equipped road vehicle. *IEEE Trans. Ind. Electron.* 63(9), 5774–5785 (2016). <https://doi.org/10.1109/tie.2016.2573239>
 23. Chen, G., Song, Y., Guan, Y.: Terminal sliding mode-based consensus tracking control for networked uncertain mechanical systems on digraphs. *IEEE Transact. Neural Networks Learn. Syst.* 29(3), 749–756 (2016). <https://doi.org/10.1109/tnnls.2016.2636323>
 24. Madani, T., Daachi, B., Djouani, K.: Modular-controller-design-based fast terminal sliding mode for articulated exoskeleton systems. *IEEE Trans. Control Syst. Technol.* 25(3), 1133–1140 (2016). <https://doi.org/10.1109/tcst.2016.2579603>
 25. Solis, C.U., Clempner, J.B., Poznyak, A.S.: Fast terminal sliding-mode control with an integral filter applied to a van der pol oscillator. *IEEE Trans. Ind. Electron.* 64(7), 5622–5628 (2017). <https://doi.org/10.1109/tie.2017.2677299>
 26. Lin, C.K.: Nonsingular terminal sliding mode control of robot manipulators using fuzzy wavelet networks. *IEEE Trans. Fuzzy Syst.* 14(6), 849–859 (2006). <https://doi.org/10.1109/tfuzz.2006.879982>
 27. Zheng, J., et al.: Robust motion control of a linear motor positioner using fast nonsingular terminal sliding mode. *IEEE ASME Trans. Mechatron.* 20(4), 1743–1752 (2014). <https://doi.org/10.1109/tmech.2014.2352647>
 28. Xu, S.S.D., Chen, C.C., Wu, Z.L.: Study of nonsingular fast terminal sliding-mode fault-tolerant control. *IEEE Trans. Ind. Electron.* 62(6), 3906–3913 (2015). <https://doi.org/10.1109/tie.2015.2399397>
 29. Lee, J., Chang, P.H., Jin, M.: Adaptive integral sliding mode control with time-delay estimation for robot manipulators. *IEEE Trans. Ind. Electron.* 64(8), 6796–6804 (2017). <https://doi.org/10.1109/tie.2017.2698416>
 30. Parra-Vega, V., et al.: Dynamic sliding PID control for tracking of robot manipulators: theory and experiments. *IEEE Trans. Robot. Autom.* 19(6), 967–976 (2003). <https://doi.org/10.1109/tra.2003.819600>
 31. Xu, Q.: Continuous integral terminal third-order sliding mode motion control for piezoelectric nanopositioning system. *IEEE ASME Trans. Mechatron.* 22(4), 1828–1838 (2017). <https://doi.org/10.1109/tmech.2017.2701417>
 32. Xu, Q.: Digital integral terminal sliding mode predictive control of piezoelectric-driven motion system. *IEEE Trans. Ind. Electron.* 63(6), 3976–3984 (2015). <https://doi.org/10.1109/tie.2015.2504343>
 33. Boiko, I., Fridman, L., Castellanos, M.: Analysis of second-order sliding-mode algorithms in the frequency domain. *IEEE Trans. Automat. Control* 49(6), 946–950 (2004). <https://doi.org/10.1109/tac.2004.829615>
 34. Utkin, V.: On convergence time and disturbance rejection of super-twisting control. *IEEE Trans. Automat. Control* 58(8), 2013–2017 (2013). <https://doi.org/10.1109/tac.2013.2251812>
 35. Wang, H., et al.: Finite-time chaos synchronization of unified chaotic system with uncertain parameters. *Commun. Nonlinear Sci. Numer. Simulat.* 14(5), 2239–2247 (2009). <https://doi.org/10.1016/j.cnsns.2008.04.015>
 36. Li, T.S., et al.: A DSC approach to robust adaptive NN tracking control for strict-feedback nonlinear systems. *IEEE Transactions on Systems, Man, and Cybernetics, Part B (cybernetics)* 40(3), 915–927 (2009)
 37. Anh, H.P.H., Nam, N.T.: Adaptive line trajectory identification of industrial 5-dof robot arm using neural mimo narx model. In: *AETA 2013: Recent Advances in Electrical Engineering and Related Sciences*, pp. 605–615. Springer (2014)
 38. Brahmi, B., et al.: Passive and active rehabilitation control of human upper-limb exoskeleton robot with dynamic uncertainties. *Robotica* 36(11), 1757–1779 (2018). <https://doi.org/10.1017/s0263574718000723>
 39. Brahmi, B., et al.: Enhancement of sliding mode control performance for perturbed and unperturbed nonlinear systems: theory and experimentation on rehabilitation robot. *Journal of Electrical Engineering & Technology* 16(1), 599–616 (2021). <https://doi.org/10.1007/s42835-020-00615-2>

How to cite this article: Brahmi, B., Rahman, M.H., Saad, M.: Impedance learning adaptive super-twisting control of a robotic exoskeleton for physical human-robot interaction. *IET Cyber-Syst. Robot.* e12077 (2023). <https://doi.org/10.1049/csy2.12077>

APPENDIX A

Let $\sigma = 0$ in Equation (17), means that $\sigma_i = 0, i = 1, \dots, n$. For $\sigma_i = 0$, we find $e = -\lambda_1 |\dot{e}_i|^\beta \text{sign}(\dot{e}_i)$. For $\dot{e}_i > 0$, we have $|\dot{e}_i|^\beta \text{sign}(\dot{e}_i) = \dot{e}_i^\beta$ and for $\dot{e}_i < 0$, we have $|\dot{e}_i|^\beta \text{sign}(\dot{e}_i) = \dot{e}_i^\beta$. We can conclude that $e = -\lambda_1 \dot{e}_i^\beta$. In light of this, we can find

$$\dot{e} = -\left(\frac{1}{\lambda_1}\right)^{\frac{1}{\beta}} (e_i)^{\frac{1}{\beta}} = -\left(\frac{1}{\lambda_1}\right)^{\frac{1}{\beta}} |e_i|^{\frac{1}{\beta}} \text{sign}(e_i) \quad (A1)$$

If we take the Lyapunov function to be given by

$$V = \frac{1}{2} \sum_{i=1}^n e_i^2 \quad (A2)$$

Derivative in time of Equation (A2) yields

$$\dot{V} = \sum_{i=1}^n e_i \dot{e}_i \quad (A3)$$

By putting Equation (A1) into (A2), we get

$$\begin{aligned}\dot{V} &= - \sum_{i=1}^n \left(\frac{1}{\lambda_1}\right)^{\frac{1}{\beta}} |e_i|^{\frac{1}{\beta}} e_i \text{sign}(e_i) \\ &= - \sum_{i=1}^n \left(\frac{1}{\lambda_1}\right)^{\frac{1}{\beta}} |e_i|^{\frac{1+\beta}{\beta}} \\ &= - \sum_{i=1}^n \left(\frac{1}{\lambda_1}\right)^{\frac{1}{\beta}} 2^{\frac{1+\beta}{2\beta}} V^{\frac{1+\beta}{2\beta}}\end{aligned}\quad (\text{A4})$$

Equation (A4) can be rewritten as follows:

$$\dot{V} + \sum_{i=1}^n v_i V^\mu \leq 0, \quad (\text{A5})$$

where $v = \left(\frac{1}{\lambda_1}\right)^{\frac{1}{\beta}} 2^{\frac{1+\beta}{2\beta}}$ and $\mu = \frac{1+\beta}{2\beta}$. So, it stands to reason that $\dot{V} \leq 0$. The settling time can be roughly calculated using Lemma 1:

$$T_s \leq \frac{V_e^{1-\mu}(e_0)}{v(1-\mu)} \quad (\text{A6})$$

Therefore, the proof is conclusive.

Remark The finite-time convergence (T_s) is controlled by the parameters $V(e_0)$ and $\frac{1}{\lambda_1}$ in (A6). Simply said, a large enough number for λ_1 guarantees a fast convergence time, and the converse is also true. In order to achieve an optimum tradeoff among transient response speed, finite-time convergence and control performance, it is necessary to fine-tune the ratios $\frac{1}{\lambda_1}$.